small methods
www.small-methods.com

Revealing Size-Dependency of Ionic Liquid to Assist Perovskite Film Formation Mechanism for Efficient and Durable Perovskite Solar Cells

Fei Wang, Kang Zhou, Xiao Liang, Xianfang Zhou, Dawei Duan, Chuangye Ge, Xintao Zhang, Yumeng Shi, Haoran Lin, Quanyao Zhu,* Liang Li,* Hanlin Hu,* and Hongyu Zhang**

Ionic liquids (ILs) are extensively utilized for the manipulation of crystallization kinetics of perovskite, morphology optimization, and defect passivation for the fabrication of highly efficient and stable devices. However, comparing ILs with different chemical structures and selecting the appropriate ILs from the many types available to enhance perovskite device performance remains a challenge. In this study, a range of ILs containing different sizes of anions are introduced as additives for assisting in film formation in perovskite photovoltaics. Specifically, ILs with various sizes significantly affects the strength of chemical interaction between ILs and perovskite composition, inducing varying degrees of conversion of lead iodide to perovskite as well as the formation of perovskite films with markedly disparate grain sizes and morphology. Theoretical calculations in conjunction with experimental measurements revealed that small-sized anion can more effectively reduce defect density by filling halide vacancies within perovskite bulk materials, resulting in suppression of charge-carrier recombination, an extended photoluminescence lifetime, and significantly improved device performance. Boosted by ILs with appropriate size, the champion power conversion efficiency of 24.09% for the ILs-treated device is obtained, and the unencapsulated devices retain 89.3% of its original efficiency under ambient conditions for 2000 h.

1. Introduction

Perovskite solar cells (PSCs) have been regarded as one of the hot candidate devices for the next-generation of photovoltaics due to the simple production process, tunable bandgap and large-area printability.[1–4] Since the pioneer perovskite solar cells with the power conversion efficiency (PCE) of 3% were reported in 2009, remarkable progress has been made for optimizing performance of PSCs and some research has achieved desirable PCEs exceeding 25% that reach the level of commercial silicon solar cells.[5,6] Among them, component engineering was first developed to regulate the efficiency and stability of devices, and single cationic compositions, methylammonium (MA)- and formamidinium (FA)-based PSCs, have been shown to operate with exceptionally high maximum efficiency of over 23% and 24%, respectively.[7] These encouraging results set the basis for the development

F. Wang, X. Liang, X. Zhou, Q. Zhu
State Key Laboratory of Advanced Technology for Materials Synthesis and Processing
School of Materials Science and Engineering
Wuhan University of Technology
Wuhan 430070, China
E-mail: cglamri@whut.edu.cn

F. Wang, K. Zhou, X. Liang, X. Zhou, D. Duan, C. Ge, H. Lin, H. Hu
Hoffman Institute of Advanced Materials
Shenzhen Polytechnic
Shenzhen 518055, China
E-mail: hanlinhu@szpt.edu.cn

Y. Shi
International Collaborative Laboratory of 2D Materials for Optoelectronics Science and Technology of Ministry of Education
Institute of Microscale Optoelectronics
Shenzhen University
Shenzhen 518060, China

X. Zhang
Department of Sports Medicine and Rehabilitation
Peking University Shenzhen Hospital
Shenzhen 518035, China
E-mail: 1182@pkuszh.com

L. Li
Department of Sciences and Engineering
Sorbonne University Abu Dhabi
Abu Dhabi 25586, UAE
E-mail: liang.li@sorbonne.ae

H. Zhang
State Key Laboratory of Supramolecular Structure and Materials
College of Chemistry
Jilin University
Changchun 130012, China
E-mail: hongyuzhang@jlu.edu.cn

The ORCID identification number(s) for the author(s) of this article can be found under https://doi.org/10.1002/smtd.202300210

DOI: 10.1002/smtd.202300210

of a family of FA-based perovskites with high efficiency and better thermal stability. However, $FAPbI_3$ is prone to transformation from its desirable trigonal black α phase to a hexagonal δ phase with a symmetric broadband gap, a process that alleviates the photoelectric performance of perovskite solar cells.[8,9] Moreover, the nucleation rate and crystal growth of $FAPbI_3$ crystals are hard to control, which decreases the quality of the $FAPbI_3$ films required for implementation in devices. A combination of cations to prepare mixed A-site formamidinium perovskites has been suggested to address these challenges.[10] Nevertheless, the easily formed defects both at the surface and in the bulk of perovskite layer are still considered as principal factor to limit the further development of PSCs and remain to be addressed.[11,12]

In order to overcome the above limitations, various types of additives, such as polymers, 2D materials, organic or inorganic salts, Lewis acids or bases and metal-organic frameworks (MOF) are selected to adjust the crystallization process of perovskite and reduce defect density.[13–16] Among these additives, ionic liquids (ILs), a class of molten salts with highlighted characteristics of excellent stability, solvate capability, structural designability, and high carrier mobility have been extensively applied in the perovskite field, especially in PSCs.[17–19] Abate and colleagues incorporated IL methylammoniumformate (MAFa) into PSCs through one-step fabrication method to achieve planar perovskite solar cell with the PCE of 19.5% in 2016.[20] The IL MAFa was found to effectively manipulate crystallization kinetics of perovskite to form high quality film with larger crystals and less defects. Li and coworkers employed the IL 1-propionate-4-amino-1,2,4-triazolium tetrafluoroborate ($PATMBF_4$) as a multifunctional additive to regulate crystal growth and passivate defects of perovskite.[21] Although many evolutions have been realized on ILs as additives to effectively reduce the defects of perovskite, assist the film-forming process and improve the performance of perovskite devices, there are few works systematically concentrating on the selection principle of ILs for perovskite devices. However, the structural diversity of ILs prompts dilemma in the selection of appropriate ILs for high-performance perovskite devices. Recently, Liu et al.[22] compared to the passivation effect between the anion HSO_4^- in ILs with I^- and Br^- through the DFT calculation results and demonstrated that HSO_4^- is more effective for defect passivation. Unfortunately, there is still a lack of specific mechanistic research on the effect of structure of ILs on assisting the crystallization of perovskite, forming high-quality films, and enhancing device performance, which is unfavorable for the continued application of ILs in the field of perovskite devices.

Here, we incorporated a series of ILs with different anions that possess distinguishing sizes as additives into the perovskite precursor solution, aiming at enhancing the photoelectric performance of PSCs. More importantly, we systematically investigated the effect of size of ionic liquid on assisting perovskite film formation, defect states, film morphology, and device performance. Specifically, the ILs with different sizes induced the varying degrees of conversion of lead iodide to perovskite and the formation of perovskite film with different grain sizes and morphology, which were verified by the grazing-incidence wide-angle scattering measurements (GIWAXS) and scanning electron microscopy (SEM). Nuclear magnetic resonance spectroscopy (NMR), X-ray photoelectron spectroscopy (XPS) analysis, and fourier-transform infrared spectroscopy (FTIR) were applied to reveal the concrete interaction of the anion and cation in ILs with perovskite and explain that the size of anions significantly affects the strength of chemical interaction. Taking advantage of small size of anion in ILs, we discovered the anion with small size can more effectively decrease the defect density through filling up the halide vacancies within the perovskite bulk materials, leading to the suppression of the charge-carrier recombination, extension of photoluminescence (PL) lifetime, and prominently enhanced device performance. Through optimizing the size of anion in ILs, the highly stable and efficient PSC with the PCE of 24.09% was achieved. Our study provides an in-depth understanding of the structural design and selection of ILs for high-efficiency solar cells and promotes the further development of ILs in photovoltaic field.

2. Results and Discussion

The traditional two-step sequential method was employed to fabricate perovskite thin film according to our reports.[23,24] The PbI_2 solution doped with Cs^+ was first deposited on the SnO_2/ITO substrate and organic salt (FAI, MABr and MACl) were then spin-coated on top of the PbI_2 layer, followed by thermal annealing to form an unmodified perovskite thin film as shown in Figure S1a (Supporting Information). For the IL-treated perovskite layer, MAFa, methylammonium acetate (MAAc), and methylammonium propionate (MAPa) were incorporated into the organic salt solution, respectively, to form MAFa, MAAc and MAPa-treated perovskite thin film and the chemical structures of MAFa, MAAc and MAPa are shown in Figure S1b (Supporting Information).

XPS was first utilized to analyze the binding energies of the element of control and IL-perovskite film and reveal the chemical interaction between ILs and perovskite composition. The characteristic XPS peaks corresponding to the element of Br, I, Pb, C, and N in **Figure 1**a and the typical O 1s peak was located at 531.80 eV corresponding to the O element in IL MAFa, MAAc, and MAPa, indicating that the existence of IL in perovskite thin film (Figure 1b). The significantly reduced content of Pb^0 in MAFa-treated, two obvious peaks of Pb 4f for the film without IL treatment (control) were located at 142.80 and 138.00 eV, which were assigned to the signals of Pb $4f_{5/2}$ and Pb $4f_{7/2}$, respectively. For the IL MAFa-treated perovskite film, the peaks of Pb $4f_{5/2}$ and Pb $4f_{7/2}$ were both shifted to lower binding energies (142.60 and 137.74 eV), indicating that the formation of chemical coordination bonds between COO^- in IL MAFa with the perovskite film. In the IL MAAc-treated perovskite film, similar phenomena were observed that the peaks of Pb $4f_{5/2}$ and Pb $4f_{7/2}$ were both shifted to 142.69 and 137.83 eV, interpreting as the chemical coordination of CH_3COO^- with Pb^{2+}. In contrast to the MAFa and MAAc, the signals of Pb $4f_{5/2}$ and Pb $4f_{7/2}$ for MAPa-treated perovskite film slightly shifted to lower binding energies (142.77 and 137.96 eV), suggesting the weaker chemical interaction between the functional groups in MAPa and Pb^{2+}. The above results showed that the size of anions in ILs will affect the interaction between ILs and perovskite composition and the coordination ability of IL with uncoordinated Pb was further compared by the proportion statistics of Pb^0 as shown in Figure 1c,d. The significantly reduced content of Pb^0 in MAFa-treated perovskite film proved the strong chemistry coordination with uncoordinated Pb^{2+} for effectively filling the organic vacancy in the perovskite film. In

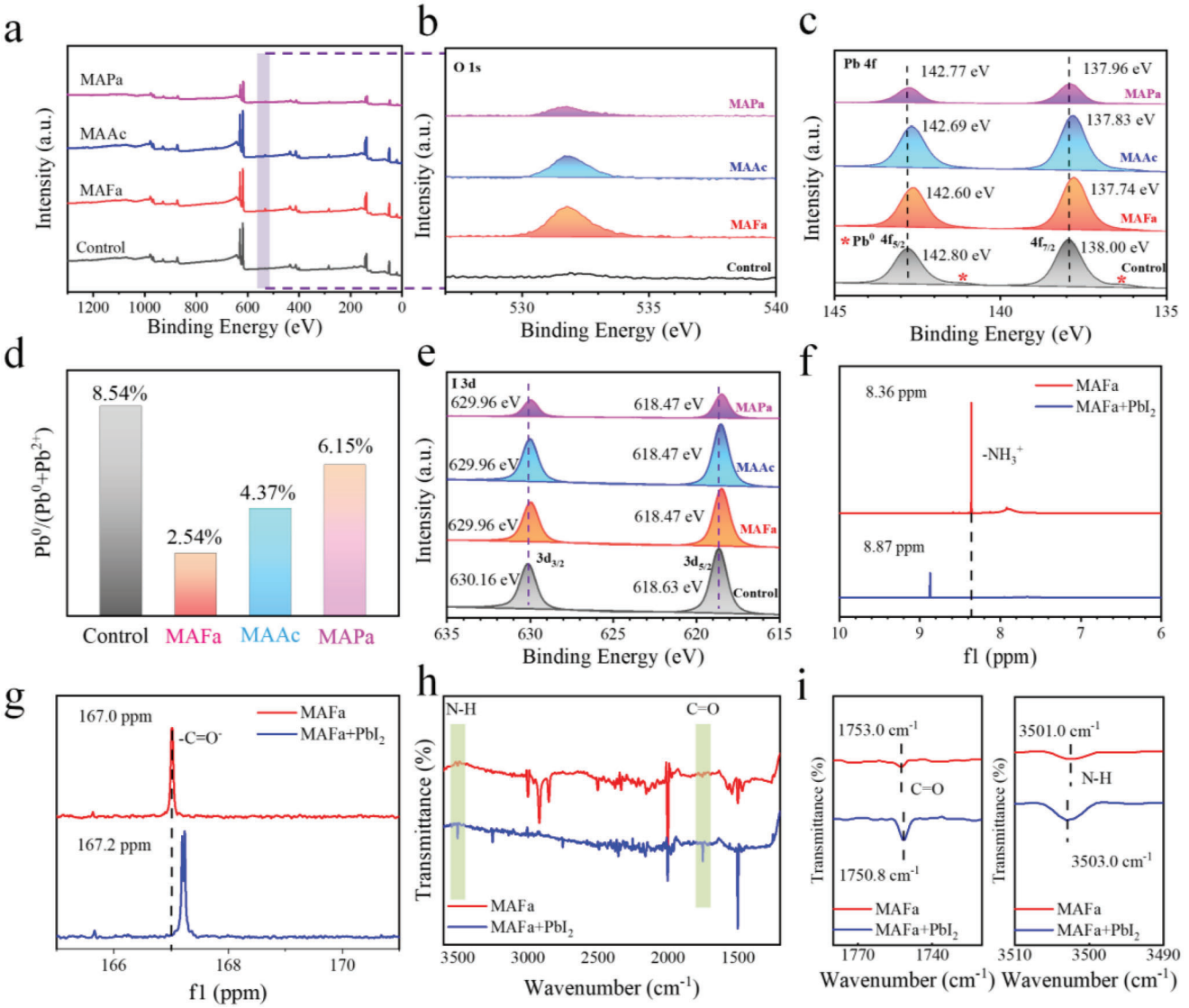

Figure 1. a) XPS spectra and the high-resolution XPS spectrum for b) O 1s and c) Pb 4f. d) The proportion statistics of Pb^0 in corresponding perovskite films from the results of high-resolution XPS spectrum for Pb 4f. e) The high-resolution XPS spectrum for I 3d from the control and ILs MAFa, MAAc, and MAPa-treated perovskite films. f) ^{1}H NMR and g) ^{13}C NMR spectra of MAFa and MAFa+PbI_2 solutions. h–i) FTIR spectra of MAFa and MAFa+PbI_2 solutions.

addition, two peaks located at 630.16 and 618.63 eV for the control perovskite films were attributed to the binding energies of I $3d_{3/2}$ and I $3d_{5/2}$ in the high-resolution XPS spectrum of I 3d, and these peaks of I 3d shifted toward a lower binding energy (629.96 and 618.47 eV) for both MAFa, MAAc, and MAPa-treated perovskite film owing to the formation of N–H···I hydrogen bonds between ILs and perovskite films.[25]

In order to further investigate the interaction between ILs and perovskite, ^{1}H NMR spectra were carried out for the MAFa and MAFa/PbI_2 solution to show that the amino hydrogen spectrum in MAFa shifted from 8.36 to 8.87 ppm owing to the strong N–H···I hydrogen bond between the MAFa and I^- (Figure 1f,g; Figure S2, Supporting Information).[8,26] Furthermore, the shift of C=O peak from 167.0 ppm for MAFa to 167.2 ppm for MAFa/PbI_2 solution in the ^{13}C NMR spectra further uncovered the interaction of the COO^- in MAFa with Pb^{2+}. To make our conclusions more convincing, these bonding interactions between MAFa and perovskite were further proven by FTIR (Figure 1h). The two characteristic peaks appeared at a wavenumber of 1753.0 and 3501.0 cm^{-1}, assigning to the signal of C–O bond and N–H bond in MAFa respectively. After the incorporation of PbI_2 in MAFa solution, the C=O vibration in MAFa shifted to 1750.8 cm^{-1}, indicating the increased vibration frequency of C=O to show that C=O bond in MAFa can donate an electron pair to the under-coordinated Pb atoms, thus forming the strong C=O–Pb chelate bond (Figure 1i). In contrast, the C=O characteristic peaks of the MAAC and MAPa samples showed a slight shift (Figure S3, Supporting Information), suggesting that the strength of the chemical interaction was related to the size of the anions. The movement of the N–H bond to 3503.0 cm^{-1} also

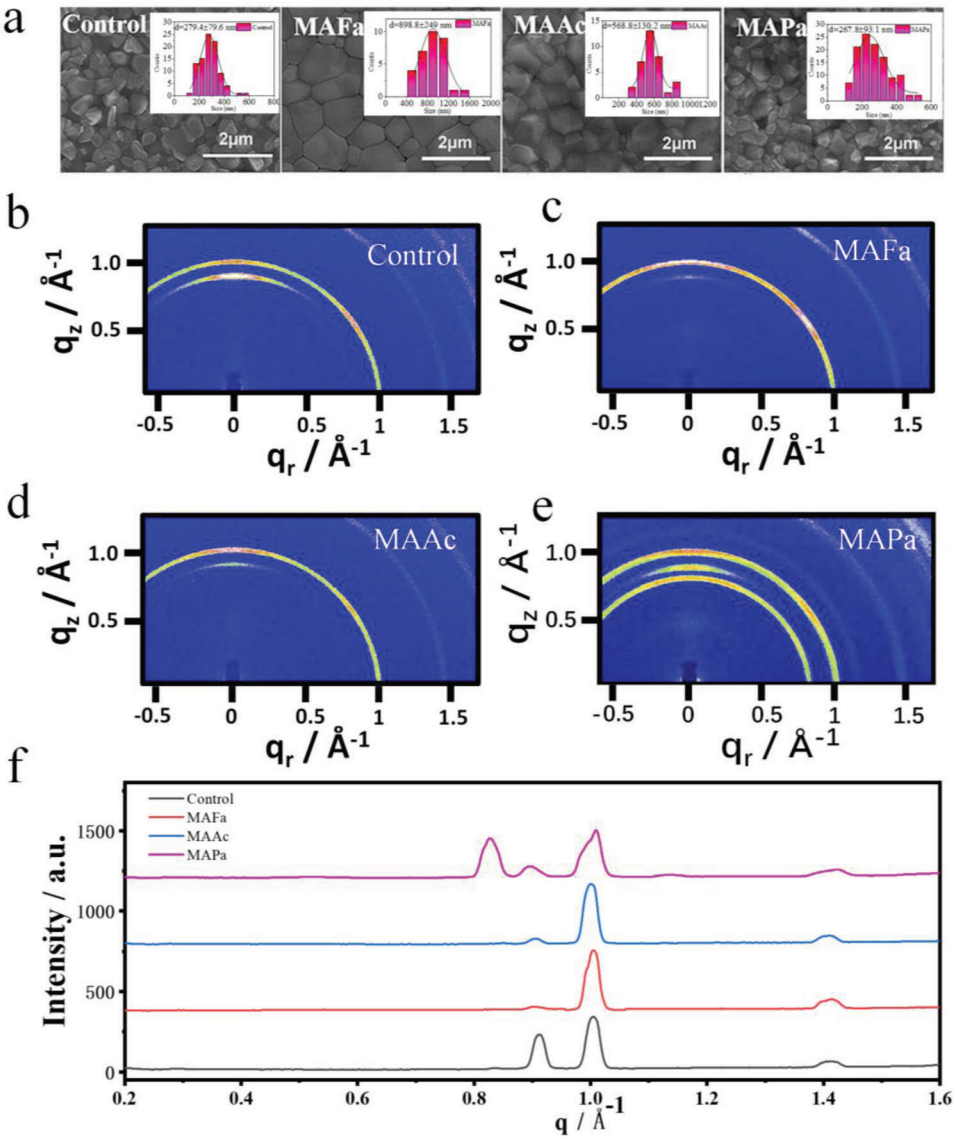

Figure 2. a) SEM images of control and ILs treated-perovskite films. The insets display the grain size distribution of the corresponding perovskite films. b–e) The 2D GIWAXS spectra of control and ILs-treated perovskite film. f) Radial integration integration of both control and ILs-treated perovskite 2D GIWAXS patterns.

revealed the existence of N–H···I hydrogen bond. The existence of interaction ILs with perovskite composition would be beneficial for the perovskite crystal growth with sufficient defect passivation, and consequently improve the device's performance.

In-depth exploring the definite effects of different size of ILs on the crystal growth and quality of perovskite film, the top-view SEM were first employed to inspect the morphology for both the control and ILs-treated perovskite films. Compared to the control perovskite film with the grain size of 279.4 ± 79.6 nm, the MAFa and MAAc IL-treated perovskite film showed a more uniform morphology with a distinct increased grain size of 898.8 ± 249 and 568.8 ± 130 nm (**Figure 2**a). In addition, relatively small grain-size perovskite was rarely detected in the MAFa and MAAc IL-treated perovskite film, effectively reducing the number of grain boundaries where easy to occur non-radiative recombination and decomposition.[27] The facilitation of the quality of the films with lager grain size was attributed to the existence of interaction between ILs and perovskite for controlling perovskite crystal growth and offer more uniform nucleation sites during the crystallization process of perovskite.[20,28,29] On the contrary, the MAPa-treated perovskite film exhibited slightly smaller grain size of 267.8 ± 93.1 nm, which showed that weak chemical interaction was inadequate to control the crystallization process and the crystal growth process of perovskite was affected by the existence of larger size ILs in perovskite for forming high-quality films.

GIWAXS were further conducted systematically to investigate the effect of ILs on assisting the formation of perovskite. Figure 2b–e presents the 2D GIWAXS patterns of the control, MAFa, MAAc, and MAPa-treated perovskite film, respectively.

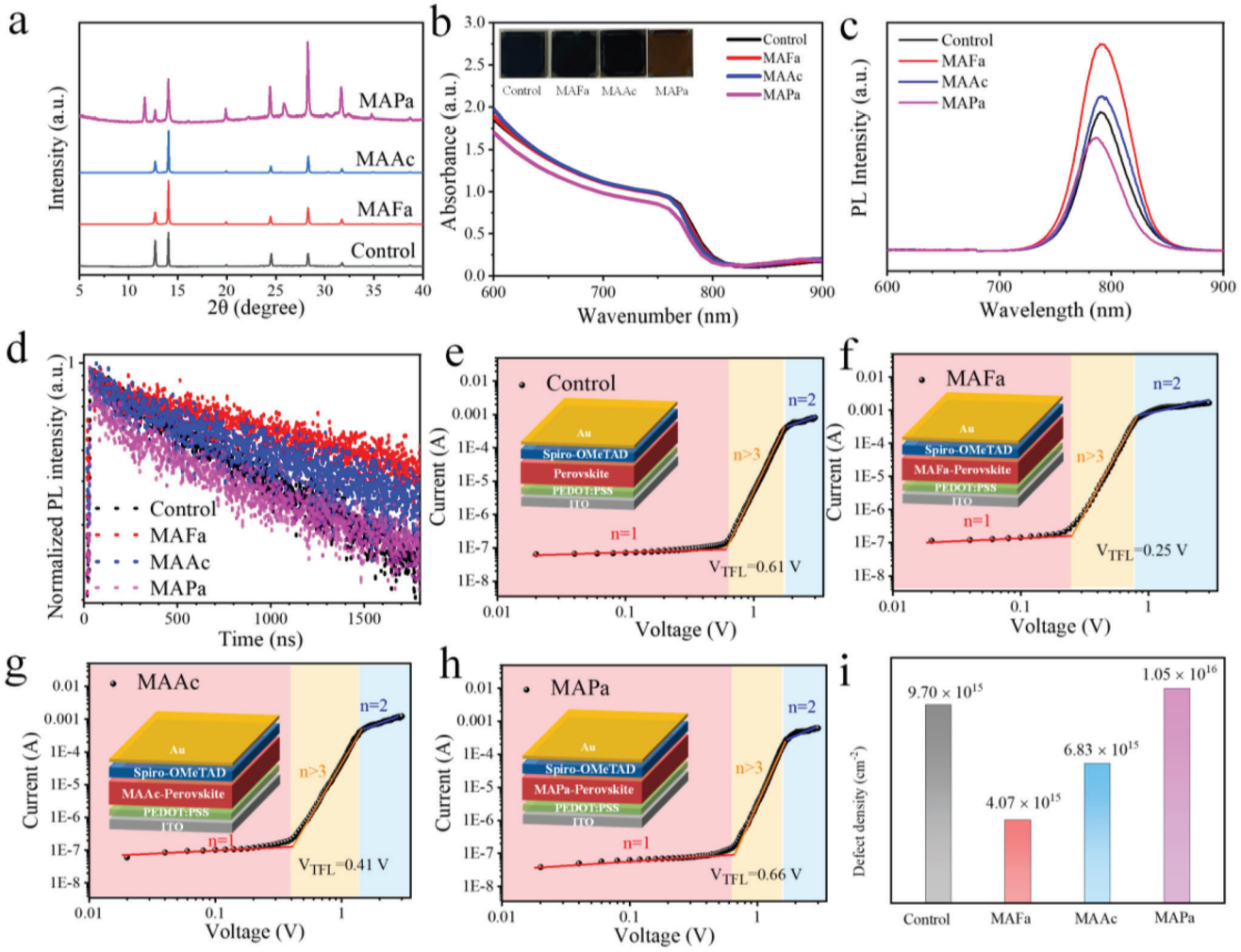

Figure 3. a) X-ray diffraction patterns of control and ILs-treated perovskite films. b) UV–vis absorption spectra of the control and ILs-treated perovskite films. c) PL and d) time-resolved PL spectra of the perovskite films. e–h) SCLC measurements of control and ILs-treated perovskite devices. i) The statistics of defect density based on the SCLC measurements.

Two scattering peaks both located at q = 0.9 and 1.0 $Å^{-1}$ appeared in the control perovskite sample and ILs-treated perovskite films, which were ascribed to the (110) of PbI_2 and the (110) of 3D perovskite crystals. However, the new scattering halos appeared in the short q regime in MAPa-treated perovskite film. According to the 2D GIWAXS data, the radial integration results for samples are plotted in Figure 2f. For the control perovskite sample, a strong peak at q = 0.9 $Å^{-1}$ belonged to signal of PbI_2, corresponding to the traditional two-step references.[30,31] By comparison, the signal of PbI_2 in MAFa and MAAc-treated perovskite samples was markedly weaker, suggesting that the addition of ILs MAFa and MAAc promoted the conversion of PbI_2 to perovskite. The additives or solvents in the perovskite precursor solution can adjust the arrangement of PbI_2 crystals through chemical interaction, so as to effectively promote the penetration of organic salts, resulting in more complete transformation to perovskite.[8,32] In the MAPa-treated perovskite film, a strong peak appeared at q = 0.8 $Å^{-1}$, which was attributed to non-perovskite phase δ-$FAPbI_3$, indicating the influence of size change on the crystallization process of perovskite.

For further investigation into the effect of the ILs on the perovskite film, X-ray diffraction (XRD) measurements were performed for control and ILs-treated perovskite films to show that the same peak appeared at ≈14.02° for both control and ILs-treated perovskite films (**Figure 3**a), suggesting the incorporation of ILs results in negligible impact on polymorphism or variation of lattice. Compared to the control film, it is worth mentioning that the intensity of peak signal of PbI_2 at 12.70° in MAFa or MAAc-treated films were significantly weaker, which were matched with the results of GIWAXS spectra. Nevertheless, a new and strong peak at 11.50° corresponding to non-perovskite phases δ-$FAPbI_3$ was observed in MAPa-treated samples to further verify that an impact on the crystallization process of perovskite was generated by IL MAPa. UV–vis absorption and PL tests were then measured to indicate the identical absorption threshold and PL peak position for control and

MAFa or MAAc-treated perovskite film, further proving maintenance of lattice in accordance with the XRD consequences (Figure 3b,c). Moreover, the reduced absorbance of MAPa-treated perovskite film (Figure 3b; Figure S4, Supporting Information) and PL intensity (Figure 3c) compared to the control film is interpreted as the formation of non-perovskite phases δ-$FAPbI_3$ and the increased defects. Interestingly, the PL intensity of the MAFa-treated film was strongest, owing to improved charge extraction/transport, reduced crystal defects, and reduced nonradiative interference. For the purpose of confirming the PL observation, time-resolved PL measurements were performed on glass/perovskites for ILs-treated and control film. Most remarkably increased PL lifetime of MAFa films were detected as shown in Figure 3d, Figure S5 and Table S1 (Supporting Information), perceived as the least nonradiative recombination loss in MAFa films.[33] The space charge-limited current (SCLC) measurements, which employed hole-only devices based on the structure of ITO/PEDOT:PSS/perovskite/Spiro-OMeTAD/Au (Figure 3e–h), were conducted to analyze the effect of ILs on the density of trap states in perovskites films. According to the following equation:

$$N_t = \frac{2\epsilon_0\epsilon_r V_{TFL}}{qL^2} \quad (1)$$

where ϵ_0 and ϵ_r represented the vacuum permittivity and the relative dielectric constant, V_{TFL} represented the onset voltage of the trap-filled limit region, q represents unit charge, and L represented layer thickness, the V_{TFL} and defect density values of control, MAFa, MAAc, and MAPa-treated perovskite films were obtained as 0.61 V (9.70×10^{15} cm^{-3}), 0.25 V (4.07×10^{15} cm^{-3}), 0.41 V (6.83×10^{15} cm^{-3}), and 0.66 V (1.05×10^{16} cm^{-3}) (Figure 3i), respectively. The induced lower defect density of MAFa-treated perovskite films was associated with the effective passivation through the existence of chemical interaction, supported by the results of XPS and NMR.

Some defects are usually prone to occur via ion migration due to the properties of ionic crystals of perovskite materials, especially at halogen defects. Density functional theory (DFT) calculations for pristine and ILs-treated perovskite materials (the computational details can be found in the Support Information) were undertaken to throw more insight into the impact of anions with different sizes in ILs (**Figure 4**a, Figure S6, Supporting Information) on halide vacancies in perovskite materials. Figure 4b,d represents the structure of a perovskite with an iodine vacancy. Trap states caused by iodide vacancy defects were often concentrated in neighboring Pb atoms toward the bottom of the conduction band (Figure 4e). In the structures of IL MAFa and MAAc-treated perovskites, MAFa and MAAc occupied the iodine vacancy, respectively, inhibiting the appearance of defect state, thus restoring the ideal electronic structures of the optimal perovskite material (Figure 4f,g). Considering the relatively large size of anions in MAPa (Figure S6, Supporting Information), which is difficult to diffuse into the perovskite lattice, and based on the known weak interaction with perovskite components and adverse effects on the crystallization process, we speculated that MAPa is not optimistic about the defect compensation, so no excessive calculations have been made here. For a more in-depth understanding of the suppression of defects by anion with different size in ILs, the relative binding affinities energy between V_I and COO^- and $HCOO^-$ were calculated as shown in Figure 4h. The calculated results revealed that the binding energy between COO^- and V_I was −5.04 eV, significantly larger than that of CH_3COO^-, demonstrating the interaction of the COO^- from IL MAFa and the V_I from the perovskite is more favorable compared to that between CH_3COO^- from IL MAAc and V_I, which resulted in exhibiting stronger ability for coordination with the undercoordinated Pb^{2+} in perovskite. Figure 4i,j showed $HCOO^-$ and CH_3COO^- treated surfaces of the perovskite, and the charge transfer occurred mostly from the Pb atom to the O atom, demonstrating strong interaction.

Based on the ILs-treated perovskite, we respectively fabricated the corresponding perovskite devices with configuration of ITO/SnO_2/control or ILs-treated perovskite/Spiro-OMeTAD/Au as shown in Figure S7 (Supporting Information). Cross-sectional SEM was first conducted for control and IL-treated cell architecture in **Figure 5**a. Obviously, different sizes of anions in ILs induced the generation of different morphologies of perovskite layers, in accordance with the top-view SEM images. Compared to the control film, the MAFa-treated perovskite layers exhibited an enlarged grain size with fewer defects. Nevertheless, numerous defects could be observed in the MAPa-treated perovskite layers, which indicated that larger anion in ILs were prejudice for the formation of high-quality films. The concentration of the ILs is then optimized as shown in Tables S2–S4 (Supporting Information) and the optimal concentration for MAFa, MAAc and MAPa both are 0.2%. The current density–voltage (J–V) curves of relevant devices were obtained at the optimum concentration in Figure 5b and the photovoltaic parameters were summarized in Table S5 (Supporting Information). The champion MAFa-treated PSC achieved the markedly enhanced efficiency of 24.09% with an open-circuit voltage (V_{OC}) of 1.181 V, a fill factor (FF) of 81.62% and a short-circuit current density (J_{SC}) of 24.99 mA cm^{-2}, whereas the control device exhibits an efficiency of only 20.62% under identical measurement situations. The J_{SC} results of MAFa-treated PSCs achieved from J–V curves agree well with the external quantum efficiency (EQE) results (24.12 mA cm^2), when integrated over the sun spectrum (Figure 5c). The anion with appropriate relative size in MAAc also promotes the efficiency of MAAc-treated PSCs to 23.01% (a V_{OC} of 1.155 V, a J_{SC} of 24.87 and an FF of 80.04%). In contrast, the larger size in MAPa resulted in deteriorated efficiency with 16.42% of MAPa-treated PSCs.

Meanwhile, the statistical findings of related performance metrics for MAFa-treated PSCs showed a significant enhancement with excellent repeatability and large efficiency fluctuations occur in MAPa-treated devices, determined by effect of ILs on formation of perovskite thin film with assistance (Figure 5d; Figure S8, Supporting Information). The steady-state PCE of champion devices of control, MAFa, MAAc, and MAPa-treated have respectively been evaluated to 20.01%, 23.74%, 22.42%, and 16.17% with stable J_{SC} of 24.11, 24.61, 24.35, and 20.74 mA cm^{-2} by maximum power point tracking, which was remarkably comparable to the results of the J–V curve (Figure 5e). The prominent improvement in photovoltaic performance accounted for the formed high-quality film with MAFa assistance and effective defect passivation with less non-radiation recombination.

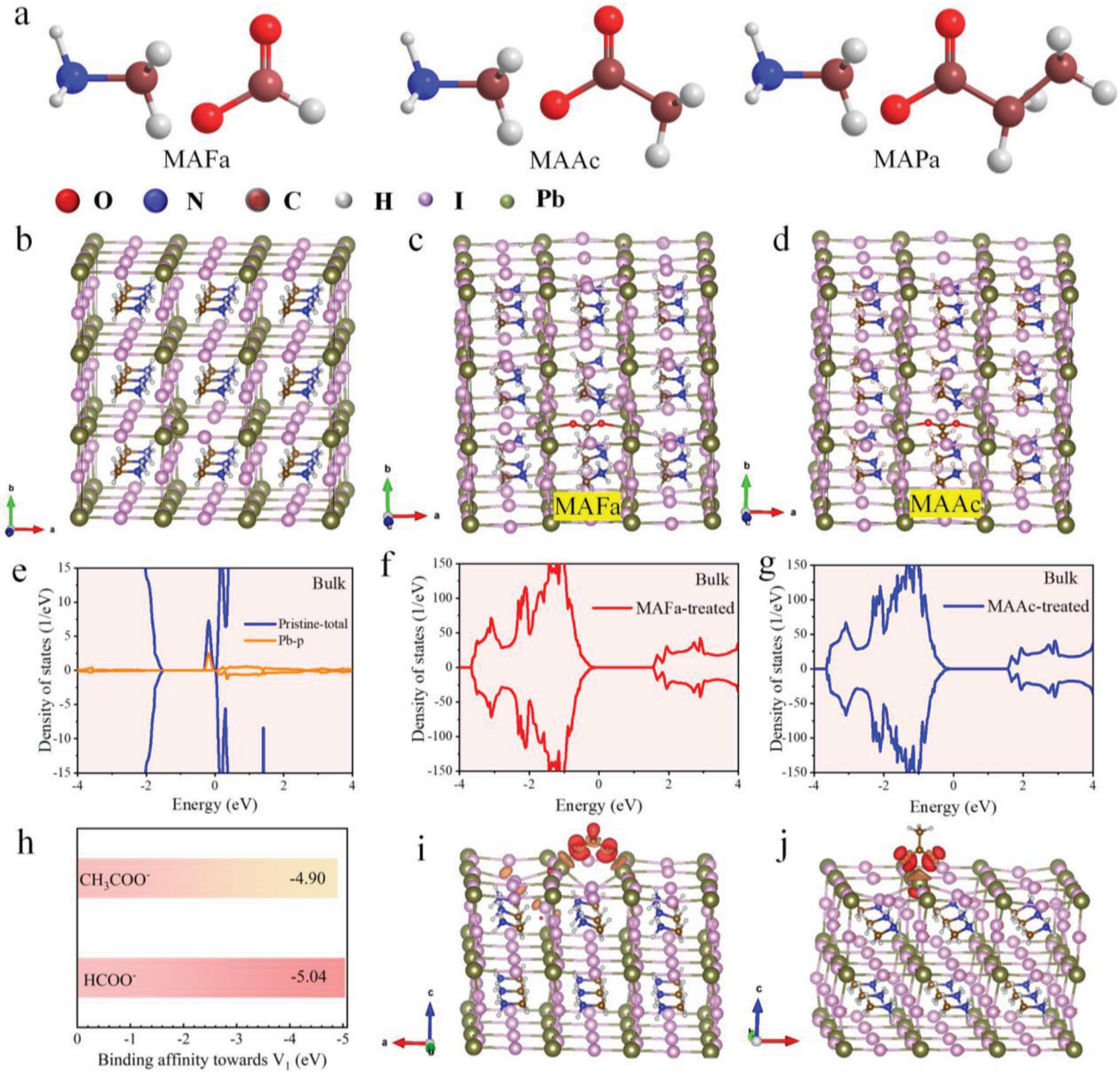

Figure 4. a) Chemical structure diagram of IL MAFa, MAAc, and MAPa. b) Crystal structure of perovskite with an iodine vacancy. c) Crystal structure of perovskite with $HCOO^-$ at the iodine vacancy site. d) Crystal structure of perovskite with CH_3HCOO^- at the iodine vacancy site. e–g) Density of states function of control, MAFa-treated and MAAc-treated crystal structure of perovskite. h) Binding affinity energy of $HCOO^-$ and CH_3HCOO^- toward the iodide vacancy site (V_I) at the perovskite bulk. i,j) Charge density of perovskite surface modified by $HCOO^-$ and CH_3HCOO^-.

To give more insight into the inhibitory effect of ILs-treated devices on nonradiative recombination, EQE_{EL} measurements for the control and ILs-treated devices are presented in Figure 5f. The EQE_{EL} values of the control, IL MAFa, MAAc, and MAPa-devices were 1.50%, 2.37%, 4.02%, and 1.04% for corresponding injection current densities, respectively. Moreover, the EL intensity of the MAFa-treated device was obviously higher than that of the control device under the identical biasing voltages of 1.35 V (Figure S9, Supporting Information). Conventional Mott-Schottky measurements were also conducted to assess the recombination and carrier transport of relevant devices as shown in Figure S10 (Supporting Information). The value of built-in potential (V_{bi}) of 0.99 V for control device, whereas that of the MAFa, MAAc, and MAPa-treated device were 1.02 V, 1.01 V, and 0.96 V according to the capacitance-voltage curve. The enhanced V_{bi} of MAFa-treated device was ascribed to boosting carriers transport and extraction, resulting in an increased V_{OC} in PSC. Furthermore, MAFa-treated PSCs exhibited the lowest dark current density, showing that IL MAFa can improve charge transfer and reduce leakage current (Figure S11, Supporting Information). The

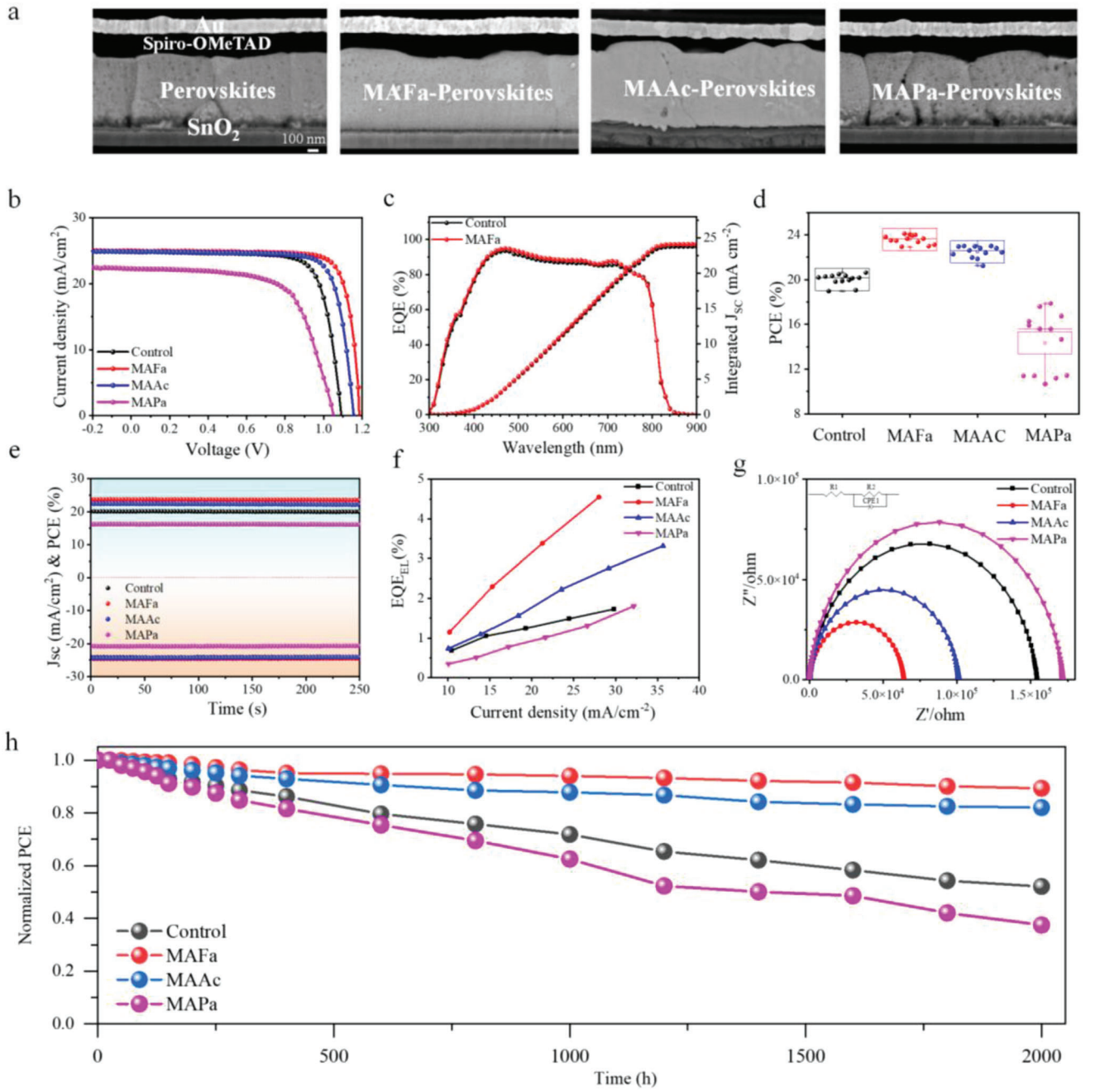

Figure 5. a) Cross-sectional SEM images of control and ILs-treated PSCs device. b) *J–V* curves of the control and ILs-treated devices. c) EQE spectra and integrated *J*sc of the control and MAFa-treated PSCs. d) The statistics of PCE of control and ILs-treated PSCs. e) Steady-state PCE and *J*sc at the maximum power point for the control and ILs-treated devices. f) EQE_{EL} of the PSCs based on control and ILs-treated versus current density. g) Nyquist plots curves of the control and ILs-treated devices. h) Normalized PCE evolution of the unencapsulated control and ILs-treated devices tracked over 2000 h at 30 °C under the RH of 25%.

impact of different ILs on the interfacial charge transport features of devices were further analyzed by electrochemical impedance spectroscopy. MAFa and MAAc-treated devices showed an arc with a smaller radius, compared to the control devices, demonstrating a decreased charge transfer resistance, nevertheless the opposite trend was observed in MAPa-treated devices. Lower charge transfer resistance indicates that photogenerated carriers may be separated more effectively, which reduced recombination and hence improves PSC performance. These results indicated that different sizes of ILs produce significant variances in carrier transport and recombination in PSCs, which markedly affected the photovoltaic performance of the devices.

The influence of ILs on the stability property of corresponding perovskite photovoltaic devices has also been systematically

examined. Previous reports verified that defects can act as pitting, causing perovskite deterioration and hence compromising device stability.[34] Interestingly, ILs were extensively applied to regulate the crystallization process of perovskite to obtain high-quality films, effectively passivate defects, and assist in forming a more hydrophobic surface, thereby suppressing the degradation of PSCs and improving device stability.[35] The water contact angles of control and target films were first obtained as shown in Figure S12 (Supporting Information) and the values of control and MAFa-treated perovskite surface were 49° and 58°, suggesting that a better moisture barrier can be acquired on MAFa-treated perovskite surface with more hydrophobicity.[36] UV–vis absorption was employed to further illustrate the enhanced stability of perovskite films by MAFa (Figure S13, Supporting Information) and small attenuation can be observed in MAFa-treated perovskite film at the storage conditions of relative humidity (RH) 50% at 25 °C after 10 days. The stability of unencapsulated devices based on corresponding perovskite films was also investigated for 2000 h at 25% ± 5% RH and room temperature. After 2000 h, MAFa-treated devices maintained 89.3% of their original PCE, whereas the control and MAPa-treated device's PCE declined to 52.1 and 37.5% under the same conditions (Figure 5h). The light-stability test was also conducted under continuous illumination of LED white light at 25 °C in ambient dry air (RH = 10 ± 5%). Noticeably, the PCE of MAFa and MAAc-treated device maintained the 85.2% and 80.4% of original efficiency, while control and MAPa-modified PSCs reduced to 72.8% and 56.8% after 600 h, respectively (Figure S14, Supporting Information). According to the above results, we could conclude that ILs with suitable size assisted in the formation of high-quality films, inhibition of ion migration and effectively passivated defects, contributing to enhancement of the stability of the films and devices.

3. Conclusion

In summary, we incorporated a series of ILs with different anion sizes as additives into the perovskite precursor solution for assisting perovskite film formation and in-depth reveal size-dependent of ionic liquids on the film morphology, defect states, and device performance. Specifically, tailoring the size of anions in ILs and thus modulating concrete chemical interaction and regulating the crystallization process, resulting in different effects for different additives. The ILs with diverse sizes caused varying degrees of conversion of lead iodide to perovskite and the fabrication of perovskite films with variable grain sizes and morphology, as measured by GIWAXS and SEM. According to the DFT calculation, the anion with small sizes in ILs are discovered to more adequately minimize defect density by filling halide vacancies within perovskite bulk materials, resulting in suppression of charge-carrier recombination, extension of photoluminescence lifetime, and significantly improved device performance, matched to the experiment results. Upon these, the ILs-treated PSCs achieve the champion PCE of 24.09% with the long-term serviceability via optimizing the size of anion in ILs. Our research fosters the ongoing development of ILs in the photovoltaic field by providing an in-depth understanding of the structural design and selection of ILs for high-efficiency solar cells.

Supporting Information

Supporting Information is available from the Wiley Online Library or from the author.

Acknowledgements

This work was supported by the Scientific Research Startup Fund for Shenzhen High-Caliber Personnel of Shenzhen Polytechnic, no. 6022310038k and 6022310049k. The financial support from the National Natural Science Foundation of China (no. 62004129 and 52173164), Shenzhen Science and Technology Innovation Commission (Project no. JCYJ20200109105003940) and Natural Science Foundation of Jilin Province (20230101038JC) is gratefully acknowledged.

Conflict of Interest

The authors declare no conflict of interest.

Data Availability Statement

Research data are not shared.

Keywords

chemical interactions, ionic liquids, perovskite solar cells, stability

Received: February 19, 2023
Revised: May 2, 2023
Published online:

[1] H. Min, D. Y. Lee, J. Kim, G. Kim, K. S. Lee, J. Kim, M. J. Paik, Y. K. Kim, K. S. Kim, M. G. Kim, T. J. Shin, S. Il Seok, *Nature* **2021**, *598*, 444.
[2] F. Wang, Y. Han, D. Duan, C. Ge, H. Hu, G. Li, *Energy Rev.* **2022**, *1*, 100010.
[3] G. Wu, R. Liang, M. Ge, G. Sun, Y. Zhang, G. Xing, *Adv. Mater.* **2022**, *34*, 2105635.
[4] J. Liu, T. Yang, Z. Xu, W. Zhao, Y. Yang, Y. Fang, L. Zhang, J. Zhang, N. Yuan, J. Ding, S. (Frank) Liu, *Small Methods* **2022**, *6*, 2201063.
[5] Y. Zhao, F. Ma, Z. Qu, S. Yu, T. Shen, H.-X. Deng, X. Chu, X. Peng, Y. Yuan, X. Zhang, J. You, *Science.* **2022**, *377*, 531.
[6] J. Jeong, M. Kim, J. Seo, H. Lu, P. Ahlawat, A. Mishra, Y. Yang, M. A. Hope, F. T. Eickemeyer, M. Kim, Y. J. Yoon, I. W. Choi, B. P. Darwich, S. J. Choi, Y. Jo, J. H. Lee, B. Walker, S. M. Zakeeruddin, L. Emsley, U. Rothlisberger, A. Hagfeldt, D. S. Kim, M. Grätzel, J. Y. Kim, *Nature* **2021**, *592*, 381.
[7] K. Wang, C. Wu, Y. Hou, D. Yang, T. Ye, J. Yoon, M. Sanghadasa, S. Priya, *Energy Environ. Sci.* **2020**, *13*, 3412.
[8] W. Hui, L. Chao, H. Lu, F. Xia, Q. Wei, Z. Su, T. Niu, L. Tao, B. Du, D. Li, Y. Wang, H. Dong, S. Zuo, B. Li, W. Shi, X. Ran, P. Li, H. Zhang, Z. Wu, C. Ran, L. Song, G. Xing, X. Gao, J. Zhang, Y. Xia, Y. Chen, W. Huang, *Science* **2021**, *371*, 1359.
[9] Y. Huang, J. Liang, Z. Zhang, Y. Zheng, X. Wu, C. Tian, Z. Zhou, J. Wang, Y. Yang, A. Sun, Y. Liu, C. Tang, Z. Chen, C. Chen, *Small Methods* **2022**, *6*, 2200933.
[10] N. J. Jeon, J. H. Noh, W. S. Yang, Y. C. Kim, S. Ryu, J. Seo, S. Il Seok, *Nature* **2015**, *517*, 476.
[11] F. Wang, P. Wai-Keung Fong, Z. Ren, H.-L. Xia, K. Zhou, K. Wang, J. Zhu, X. Huang, X.-Y. Liu, H. Wang, Y. Shi, H. Lin, Q. Zhu, G. Li, H. Hu, *J Energy Chem* **2022**, *73*, 599.

[12] X. Yi, Y. Mao, L. Zhang, J. Zhuang, Y. Zhang, N. Chen, T. Lin, Y. Wei, F. Wang, J. Wang, C. Li, *Small Methods* **2021**, *5*, 2000441.
[13] X. Liang, X. Zhou, C. Ge, H. Lin, S. Satapathi, Q. Zhu, H. Hu, *Org. Electron.* **2022**, *106*, 106546.
[14] Y. Miao, Z. Wang, C. Chen, X. Ding, M. Zhai, L. Liu, Z. Xia, H. Wang, M. Cheng, *Sol. RRL* **2022**, *6*, 2200364.
[15] Y. Wang, W. Li, T. Zhang, D. Li, M. Kan, X. Wang, X. Liu, T. Wang, Y. Zhao, *Small Methods* **2020**, *4*, 1900511.
[16] J. Chen, N. Park, *Small Methods* **2021**, *5*, 2100311.
[17] F. Wang, C. Ge, D. Duan, H. Lin, L. Li, P. Naumov, H. Hu, *Small Struct.* **2022**, *4*, 2200048.
[18] F. Wang, X. Zhou, X. Liang, D. Duan, C.-Y. Ge, H. Lin, Q. Zhu, L. Li, H. Hu, *Adv. Energy Sustain. Res.* **2022**, *4*, 2200140.
[19] S. Bai, P. Da, C. Li, Z. Wang, Z. Yuan, F. Fu, M. Kawecki, X. Liu, N. Sakai, J. T. W. Wang, S. Huettner, S. Buecheler, M. Fahlman, F. Gao, H. J. Snaith, *Nature* **2019**, *571*, 245.
[20] J. Y. Seo, T. Matsui, J. Luo, J. P. Correa-Baena, F. Giordano, M. Saliba, K. Schenk, A. Ummadisingu, K. Domanski, M. Hadadian, A. Hagfeldt, S. M. Zakeeruddin, U. Steiner, M. Grätzel, A. Abate, *Adv. Energy Mater.* **2016**, *6*, 1600767.
[21] T. Li, S. Wang, J. Yang, X. Pu, B. Gao, Z. He, Q. Cao, J. Han, X. Li, *Nano Energy* **2021**, *82*, 105742.
[22] Y. Du, Q. Tian, X. Chang, J. Fang, X. Gu, X. He, X. Ren, K. Zhao, S. Liu, *Adv. Mater.* **2022**, *34*, 2106750.
[23] F. Wang, C. Ge, X. Zhou, X. Liang, D. Duan, H. Lin, Q. Zhu, H. Hu, *Crystals* **2022**, *12*, 815.
[24] C. Ge, J. F. Lu, M. Singh, A. Ng, W. Yu, H. Lin, S. Satapathi, H. Hu, *Sol. RRL* **2022**, *6*, 2100879.
[25] J. Ran, H. Wang, W. Deng, H. Xie, Y. Gao, Y. Yuan, Y. Yang, Z. Ning, B. Yang, *Sol. RRL* **2022**, *6*, 2200176.
[26] X. Wang, X. Ran, X. Liu, H. Gu, S. Zuo, W. Hui, H. Lu, B. Sun, X. Gao, J. Zhang, Y. Xia, Y. Chen, W. Huang, *Angew. Chemie – Int. Ed.* **2020**, *59*, 13354.
[27] Q. Zhou, Y. Gao, C. Cai, Z. Zhang, J. Xu, Z. Yuan, P. Gao, *Angew. Chemie – Int. Ed.* **2021**, *60*, 8303.
[28] R. Xu, H. Dong, P. Li, X. Cao, H. Li, J. Li, Z. Wu, *ACS Appl. Mater. Interfaces* **2021**, *13*, 33218.
[29] G. Li, Z. Su, M. Li, F. Yang, M. H. Aldamasy, J. Pascual, F. Yang, H. Liu, W. Zuo, D. Di Girolamo, Z. Iqbal, G. Nasti, A. Dallmann, X. Gao, Z. Wang, M. Saliba, A. Abate, *Adv. Energy Mater.* **2021**, *11*, 2101539.
[30] Q. Jiang, Z. Chu, P. Wang, X. Yang, H. Liu, Y. Wang, Z. Yin, J. Wu, X. Zhang, J. You, *Adv. Mater.* **2017**, *29*, 1703852.
[31] Q. Jiang, Y. Zhao, X. Zhang, X. Yang, Y. Chen, Z. Chu, Q. Ye, X. Li, Z. Yin, J. You, *Nat. Photonics* **2019**, *13*, 460.
[32] Q. Liu, Z. Ma, Y. Li, G. Yan, D. Huang, S. Hou, W. Zhou, X. Wang, J. Ren, Y. Xiang, R. Ding, X. Yue, Z. Du, M. Zhang, W. Zhang, L. Duan, Y. Huang, Y. Mai, *Chem. Eng. J.* **2022**, *448*, 137676.
[33] J. Xu, J. Cui, S. Yang, Y. Han, X. Guo, Y. Che, D. Xu, C. Duan, W. Zhao, K. Guo, W. Ma, B. Xu, J. Yao, Z. Liu, S. Liu, *Nano-Micro Lett.* **2022**, *14*, 7.
[34] F. Wang, D. Duan, M. Singh, C. M. Sutter-Fella, H. Lin, L. Li, P. Naumov, H. Hu, *Energy Environ. Mater.* **2022**, e12435, https://doi.org/10.1002/eem2.12435.
[35] S. Akin, E. Akman, S. Sonmezoglu, *Adv. Funct. Mater.* **2020**, *30*, 2002964.
[36] J. Kruszyńska, F. Sadegh, M. J. Patel, E. Akman, P. Yadav, M. M. Tavakoli, S. K. Gupta, P. N. Gajjar, S. Akin, D. Prochowicz, *ACS Appl. Energy Mater.* **2022**, *5*, 13617.